Accumulation of mutant lamin A causes progressive changes in nuclear architecture in Hutchinson–Gilford progeria syndrome

Robert D. Goldman*[†], Dale K. Shumaker*, Michael R. Erdos[‡], Maria Eriksson[§], Anne E. Goldman*, Leslie B. Gordon[¶‖], Yosef Gruenbaum**, Satya Khuon*, Melissa Mendez*, Renée Varga[‡], and Francis S. Collins[‡]

*Department of Cell and Molecular Biology, Northwestern University Feinberg School of Medicine, 303 East Chicago Avenue, Chicago, IL 60611; [‡]Genome Technology Branch, National Human Genome Research Institute, National Institutes of Health, 50 South Drive, MSC 8004, Bethesda, MD 20892-8004; [§]Department of Medical Nutrition, Karolinska Institutet, Novum, Halsovagen 7, Hiss E, Plan 6, 141 57 Huddinge, Sweden; [¶]Department of Anatomy and Cellular Biology, Tufts University School of Medicine, 136 Harrison Avenue, Stearns Building 610, Boston, MA 02111; [‖]Department of Pediatrics, Rhode Island Hospital, Providence, RI 02903; and **Department of Genetics, Institute of Life Sciences, Hebrew University of Jerusalem, Jerusalem 91904, Israel

Hutchinson–Gilford progeria syndrome (HGPS) is a premature aging disorder, commonly caused by a point mutation in the lamin A gene that results in a protein lacking 50 aa near the C terminus, denoted LAΔ50. Here we show by light and electron microscopy that HGPS is associated with significant changes in nuclear shape, including lobulation of the nuclear envelope, thickening of the nuclear lamina, loss of peripheral heterochromatin, and clustering of nuclear pores. These structural defects worsen as HGPS cells age in culture, and their severity correlates with an apparent increase in LAΔ50. Introduction of LAΔ50 into normal cells by transfection or protein injection induces the same changes. We hypothesize that these alterations in nuclear structure are due to a concentration-dependent dominant-negative effect of LAΔ50, leading to the disruption of lamin-related functions ranging from the maintenance of nuclear shape to regulation of gene expression and DNA replication.

Hutchinson–Gilford progeria syndrome (HGPS) is a premature aging disease of children. It has been considered to be a model for studying the mechanisms responsible for normal aging (1–3). Manifestations of HGPS typically appear before 24 months of age (Progeria Research Foundation's medical and research database, www.progeriaresearch.org; also see www.genereviews.org), and include loss of subcutaneous fat, severe growth retardation, hair loss, bone deformations, osteoporosis, delayed dentition, joint stiffness, hip dislocations, sclerodermatous areas, and progressive arteriosclerosis. HGPS patients have an aged appearance, and in the final stages of disease, most children have hypertension, angina, and dilated hearts because of atherosclerotic heart disease. Children with HGPS generally die of myocardial infarction or cerebrovascular accident at an average age of 13 yr (4, 5).

Mutations causing HGPS have been identified in the human nuclear lamin A (*LMNA*) gene (6, 7). Lamins are type V intermediate filament proteins and have a short N-terminal "head" domain, an α-helical "central rod" domain, and a globular tail domain (8). Lamins are classified as either A or B type according to their primary sequence, expression pattern, and biochemical properties. B-type lamins are expressed in all cells during development and in adult animals, whereas A-type lamins are expressed in differentiated cells. The *LMNA* gene encodes three A-type lamins: lamin A (LA), lamin C, and lamin AΔ10 (8). Lamin A contains a C-terminal CAAX box, which undergoes methyl esterification and farnesylation. In the process of LA maturation, the C-terminal 18 residues, which include the modified C-terminal cysteine, are removed in two specific cleavage steps (9). The basic building block of lamin structures is a dimer that is formed through parallel and in-register coil–coil interactions between rod domains. These dimers associate in a head-to-tail fashion to form protofilaments that associate laterally to form higher-order structures (10). These structures are the major components of the nuclear lamina, a complex molecular interface located between the inner membrane of the nuclear envelope and chromatin. The lamins are also distributed throughout the nucleoplasm and are involved in numerous functions, including DNA replication, transcription, chromatin organization, nuclear positioning and shape, as well as the assembly/disassembly of the nucleus during cell division (8).

The most frequent *LMNA* mutation (6) in HGPS is a nucleotide substitution at position 1824, C → T, which does not cause an amino acid change (G608G) but partially activates a cryptic splice site, deleting 150 nt in exon 11. This predicts a 50-aa deletion near the C terminus. Low levels of both the mutant mRNA and the mutant protein, LAΔ50, are expressed in fibroblasts derived from HGPS patients (6). In addition, HGPS cell nuclei frequently display irregular shapes (6). Similar nuclear shape abnormalities have been reported in patients with other *LMNA* mutations, which have been linked to other "laminopathies" such as Emery–Dreifuss muscular dystrophy, dilated cardiomyopathy-1A, Dunnigan-type familial partial lipodystrophy, mandibuloacral dysplasia, and atypical Werner's syndrome (8, 11).

In this study we examine the nuclear structural changes caused by the LAΔ50 mutation. This mutant protein was assayed both in cells derived from HGPS patients and in normal cells transfected with HGPS LAΔ150 cDNA. The results support our hypothesis that the expression of LAΔ50 has an age-dependent, cumulative, and ultimately devastating effect on nuclear architecture and function, which is responsible for premature aging in patients with HGPS.

Materials and Methods

Cell Culture. Fibroblasts from HGPS patients carrying the 1824 C → T mutation were obtained from the NIA Aging Cell Culture Repository, Coriell Institute for Medical Research (AG11513; Camden, NJ) and The Progeria Research Foundation (HGADFN003; Peabody, MA). Fibroblasts from unaffected older adults (AG09602B derived from a 92-yr-old female; Coriell) and unaffected human infant foreskin fibroblasts (Coriell) were used as controls. Cells were grown in MEM with Earle's salts (Invitrogen/GIBCO), 15% FCS (HyClone), 50 units/ml penicillin, and 50 μg/ml streptomycin (Invitrogen/GIBCO) in 60-mm culture dishes. When cells reached confluence, they were trypsinized and subcultured. The passage number of

CELL BIOLOGY

each cell type was recorded. HeLa cells were grown in DMEM (Invitrogen/GIBCO) with 10% calf serum and antibiotics.

Preparation of Plasmids for Bacterial Expression and Transfection Studies. The pEGFP-myc-LA vector (12) was converted into the LAΔ50 mutant cDNA (6). The pEGFP-myc-LA vector was digested with *Asc*I and *Xba*I, removing the 3′ 1.977 kb of the LA insert. The LAΔ150 mutation was introduced as an RT-PCR product from the HGPS cell line, AG01972 (Coriell) (6), including an *Xba*I restriction site downstream of the LA termination codon by using the primers (5′-ACTCCGAGCAGTCTC-TGTCC-3′ and 5′-GGTCCTCTAGATTACATGATGCTG-CAGTTCTG-3′), digested with *Asc*I and *Xba*I, gel purified, and ligated to the vector. Colonies were screened by PCR and verified by complete sequencing (data not shown).

The bacterial expression and purification of WT and mutant LA proteins were carried out as described in refs. 13 and 14. For this purpose pET24-LA and pET24-LAΔ150 plasmids containing a T7 tag were constructed. We subcloned WT LA from pET-LA (13) by PCR and inserted the fragment between the *Bam*HI and *Sal*I restriction sites in the pET24 vector (Novagen) (pET24-LA). Then pET24-LAΔ150 was prepared as above.

Fluorescence and Electron Microscopy. Indirect immunofluorescence was carried out as described in ref. 12. Cells grown on coverslips were fixed with either formaldehyde followed by a brief treatment with 0.05% IGEPAL CA-630 (Nonidet P-40) or cold methanol (−20°C). The fixed cells were rinsed in PBS and overlaid with primary Abs. These Abs included a rabbit anti-LA (no. 266) and a rat anti-LA (no. 270) (15); a nucleoporin Ab (mAb414, Covance, Princeton) (16); a rabbit anti-human NUP153 (a gift of K. Ullman, University of Utah, Salt Lake City) (17); a rabbit anti-human emerin (a gift of K. Wilson, The Johns Hopkins University, Baltimore); a rabbit anti-pre-LA, which was generated against 14 amino acids (647–660) of pre-LA (a gift of S. Young, University of California, San Francisco); a mouse mAb directed against proliferating cell nuclear antigen (PC-10, Santa Cruz Biotechnology); and a mouse anti-T7 tag mAb (Novagen). Secondary Abs included lissamine rhodamine-conjugated donkey anti-rabbit IgG (Jackson ImmunoResearch); fluorescein-conjugated or Alexa 488-conjugated goat anti-rabbit and goat anti-mouse IgGs (Molecular Probes); Alexa 568 goat anti-rat and goat anti-rabbit IgG (Molecular Probes); and horseradish peroxidase-conjugated donkey anti-rat (Jackson ImmunoResearch). Cells were observed with an LSM510 confocal microscope (Zeiss).

For live-cell observations, GFP-LA constructs were introduced into HeLa cells by electroporation as described in ref. 12. Cells were transfected with either pEGFP-myc-LA or pEGFP-myc-LAΔ150 and plated onto coverslips. These coverslips were transferred 24–72 h later into a live-cell imaging chamber (Bioptechs, Butler, PA) containing Leibovitz's L15 medium (Invitrogen/GIBCO) with 10% FCS and antibiotics (12). The cells were then examined with an LSM510 confocal microscope (Zeiss) equipped with a stage/objective temperature controller (18). For fluorescence recovery after photobleaching (FRAP), a region of interest was photobleached and the nucleus was imaged every 30 min, as described in ref. 12.

For microinjection studies, human foreskin fibroblasts were grown on locator coverslips (Bellco, Vineland, NJ) and injected at a concentration of 1–2 mg/ml of bacterially expressed T7-LA or T7-LAΔ50 in injection buffer (see ref. 12 for details). The cells were fixed at 30–35 min after injection, processed for indirect immunofluorescence, and located as described in ref. 19. For transmission electron microscopy, cells in tissue culture dishes were fixed, embedded in plastic, and processed for thin sectioning as described in ref. 20.

Morphometric Analysis. To determine the overall percentage of lobulated or misshapen nuclei in cells at different passage numbers, 200 nuclei were scored either as lobulated, if they contained more than two lobulations, or not lobulated. These determinations were made by using a double-blind approach, followed by averaging the two data sets.

To analyze the changes in nuclear shape, we measured the perimeter and the area of nuclei in both AG09602B and HGADFN003 cells at different passages. This measurement was carried out on the midsection of the nucleus by using the overlay/measure function in the LSM software (Zeiss). To determine the extent of nuclear lobulation, we measured 50–200 randomly selected nuclei per passage and calculated the nuclear roundness or contour ratio ($4\pi \times$ area/perimeter^2) (21). The contour ratio for a circle is 1. As the nucleus becomes more lobulated, this ratio approaches 0. To calculate the perimeter length and area, we traced the outline of nuclei with a closed loop drawing tool by using images captured from cells prepared for immunofluorescence with LA Ab. We included lamin fluorescence that was associated with the edge of the lobulations and deep invaginations that typified the surface of later-passage HGPS cells. To determine the significance of these observations we used a two-tailed Student t test.

Western Blotting. To prepare whole-cell extracts from HGADFN003 cells, we seeded two 60-mm culture dishes at the same time. When they reached confluence, one dish was trypsinized and cells were counted by using a hemacytometer to estimate cell number in the second plate. SDS-sample buffer was added to the other dish to prepare whole-cell protein, which was separated by SDS/7.5% PAGE in a Bio-Rad Protean II system and then transferred to BA85 nitrocellulose (Schleicher & Schull). Nonspecific epitopes were blocked with 10% nonfat dry milk; the membrane was reacted with rat anti-human LA/C, washed with PBS/0.5% Tween 20, and subsequently reacted with a horseradish peroxidase-conjugated Ab. Ab binding was visualized by using the SuperSignal West Pico Chemiluminescent Substrate System (Pierce) on a Kodak Image Station 440.

Results

In a previous study it was shown that 48% of the HGPS fibroblasts expressing the common 1824 C → T LA mutation had misshapen or lobulated nuclei (6). We were intrigued by this observation because presumably all HGPS cells expressed the LAΔ50 mutant protein. In an attempt to gain new insights into this variation in nuclear morphology, we initiated a detailed study of HGADFN003 cells obtained from a 2-yr-old HGPS patient with the 1824 C → T mutation. During early passages, the nuclei appeared relatively normal with respect to their overall morphological features as shown by immunofluorescence with LA Ab. For example, in passage 6 cells, only 31.3% were lobulated, as defined by the presence of more than two lobulations at their surfaces (Fig. 1; see *Materials and Methods*). When this same definition was used, the number of misshapen nuclei increased to 53.7% by passage 13 and 80.9% by passage 26 (Fig. 1). There was also an apparent increase in thickness and prominence of the lamina coincident with nuclear shape changes (compare Fig. 1 *a* and *c*). In normal human foreskin fibroblasts <8% of the nuclei appeared lobulated up to passage 17 (Fig. 1*d* and data not shown). The same was true for passage 2 cells (AG09602B) from a normal 92-yr-old. By passage 17, however, 22.1% of these latter cells contained misshapen nuclei (Fig. 1). Even though there were increases in nuclear lobulations in these control cells, we never observed nuclei that were as severely misshapen as those seen in the majority of HGPS cells between passages 13 and 26. Using a more quantitative approach, we calculated the average contour ratio of HGPS and control nuclei stained with LA Ab (see *Materials and Methods*). We found a
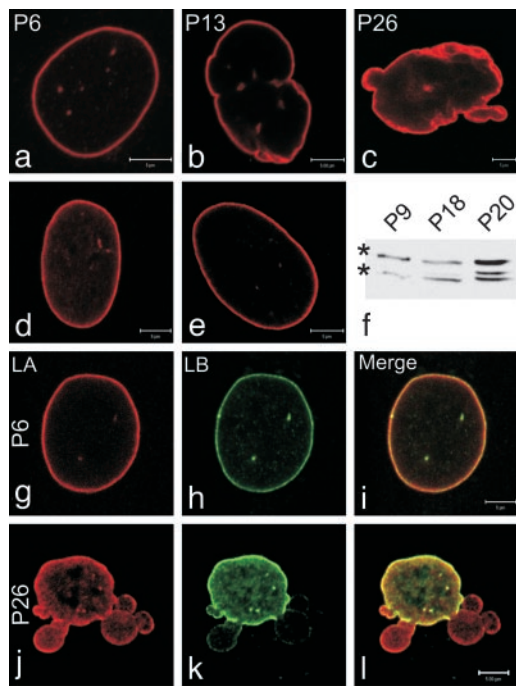
Fig. 1. Changes in nuclear architecture as HGPS cells age in culture. Typical nuclei from HGPS cells in passages 6 (*a*), 13 (*b*), and 26 (*c*), normal aged human AG09602B (*d*), and foreskin fibroblast (*e*) controls after labeling with LA Ab. Nuclei in control cells appeared similar from passage 6 through passage 17. The lamina increased in prominence or thickness in HGPS cell nuclei by passage 26 (*c*). Earlier passage HGPS (*a*) and control cell nuclei (*d* and *e*) were normal in appearance. Passage 6 and 26 HGPS cells were double labeled with LA (*g* and *j*) and LB (*h* and *k*) Abs. Note the extensive coincidence in the staining patterns in the merged image at passage 6 (*i*) and the decrease in this coincidence in a cell by passage 26 (*l*). The table shows that the contour ratio decreased as a function of passage number in HGADFN003 cells. *P* values were calculated relative to passage 2 of the AG09602B fibroblasts. There was no significant change in the contour ratio in control cells between passages 2 and 17. In HGADFN003 whole-cell extracts immunoblotted with LA/C Abs, a band migrating between LA (upper band, ∗) and lamin C (lower band, ∗) was observed and became more prominent as the passage number increased (*f*). (Scale bars = 5 μm.)

significant decrease in the contour ratio from 0.82 to 0.67 in HGPS nuclei between passages 6 and 13, and an even more significant change when comparing passages 6 and 26 (from 0.82 to 0.44) (Fig. 1, table). These changes in contour ratio reflect a 2.15-fold increase in perimeter length and a 1.54-fold increase in the mid-plane cross-sectional area (data not shown; see *Materials and Methods*). In contrast, the contour ratio remained essentially the same in control cells between passages 2 and 17 (Fig. 1 and data not shown). Because LAΔ50 is expressed in HGPS cells (6), we hypothesized that the significant changes in nuclear shape were correlated with increases in the amount of this mutant protein as the cells were passaged. Immunoblotting analyses of early- and late-passage HGPS cell extracts, using an LA Ab, showed increases in bands of the expected molecular weights for LAΔ50, LA and lamin C (Fig. 1*f*) (6).

We also examined the overall organization of lamin B1 (LB) in HGPS and control cells. Both LA and LB colocalized in early- to mid-passage HGPS cells (Fig. 1 *g–i*) and in control cells (data
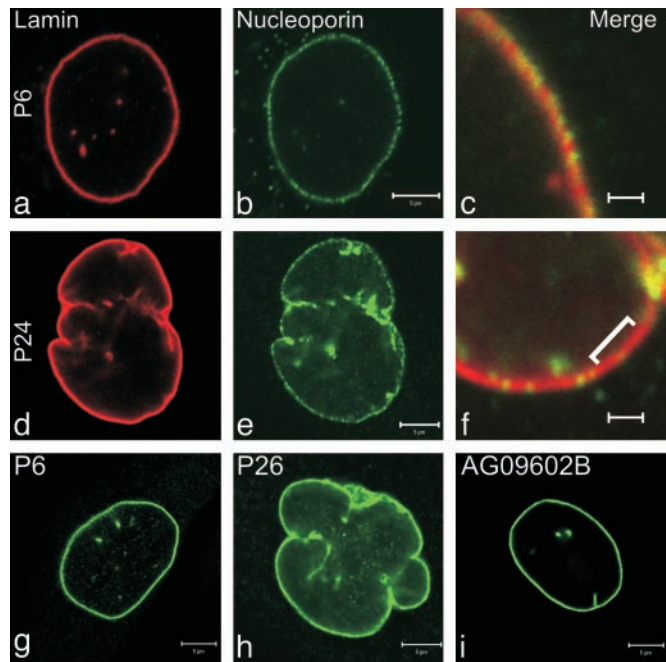

Fig. 2. Organization of nuclear pores and membranes in HGPS cells. The distribution and organization of nuclear pore complexes in a passage 6 HGPS cell (HGADFN003; *a–c*) was very similar to control AG09602B cells (not shown), as determined by double-label indirect immunofluorescence with LA and mAb 414 Abs. The typical punctate nuclear pore staining pattern along the nuclear envelope is evident. In the misshapen nuclei typifying passage 24 (*d* and *e*), the nuclear pores were frequently aggregated into large masses as detected with NUP153 Ab. Comparison of enlarged views of small regions (*c* and *f*) showing that the pores were not uniformly distributed in the nuclei of passage 26 HGPS cells (*f*); bracket in *f* shows an area that was essentially free of nucleoporins as detected by mAb414. In HGADFN003 cells stained with emerin Ab, emerin remained associated with the nuclear envelope throughout all passages (*g* and *h*). Emerin distribution appeared normal in control AG09602 cells at all passages (*i*). [Scale bars = 5 μm (*b*, *e*, and *g–i*) and 1 μm (*c* and *f*).]

not shown). However, in the highly lobulated nuclei of late-passage HGPS cells, some lobules containing a rim of LA showed little or in some cases no LB staining (Fig. 1 *j–l*). This type of segregated distribution of LA and LB1 was not detected in control cells, even in the latest passages. We also looked for alterations in other nuclear envelope components. For example, the organization of nuclear pores was determined by immunofluorescence with the nucleoporin Abs, NUP153 and 414. In early passage HGPS cells, and in control cells at all passages, both Abs showed that pores were distributed normally over the nuclear surface (Fig. 2 *a–c* and data not shown). However, the distribution of pores was significantly altered in most later-passage HGPS nuclei, as evidenced by the staining of large bright masses, many of which were associated with the clefts formed in extensively lobulated regions of the envelope (Fig. 2 *d* and *e*). In addition, there were numerous long stretches of lamina staining without pores, especially in the lobules of HGPS nuclei (see bracket in Fig. 2*f*). In contrast, the inner nuclear envelope integral membrane protein, emerin, remained localized at the nuclear surface at all passages (Fig. 2 *g–i*). This observation is in contrast to the findings in other laminopathies in which emerin is not present in nuclear lobulations or is redistributed from the nucleus to the endoplasmic reticulum (22–24).

Ultrastructural analyses of passage 6 HGPS cells, passage 2 AG09602 cells, and early-passage foreskin fibroblasts demonstrated that all had normal nuclear shapes. In addition, the organization of nuclear envelope-associated structures (including pores and peripheral heterochromatin and an extremely thin
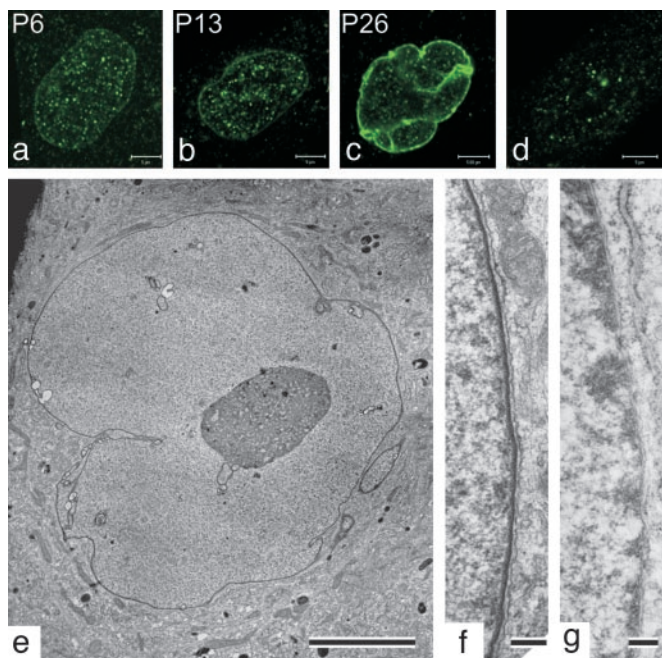
CELL BIOLOGY

Fig. 3. Pre-LA accumulation in the nuclei of HGPS cells. In passage 6 and 13 HGPS cells, the pre-LA pattern consisted of weakly staining nucleoplasmic foci (*a* and *b*) similar to control AG09602B fibroblasts (*d*). However, by passage 26, the pre-LA staining was much more intense in the lobulated nuclei and was primarily associated with the lamina region (*c*). (*e*–*g*) Electron microscopic observations of passage 26 HGPS HGADFN003 cells (*e* and *f*) and normal human foreskin fibroblasts (*g*). A high-magnification view of the nuclear envelope in a normal human foreskin fibroblast showed a normal array of heterochromatin adjacent to the nuclear envelope, making any lamina structure difficult to detect (*g*). A low-magnification view of a passage 26 HGADFN003 nucleus showed extensive lobulation (*e*). A higher-magnification view of a passage 26 cell showed a loss of peripheral heterochromatin and a prominent electron-dense lamina region associated with the inner nuclear envelope membrane (*f*). In *f* and *g*, the nucleus is to the left. [Scale bars = 5 μm (*a*–*e*) and 200 nm (*f* and *g*).]

lamina) appeared normal (Fig. 3*g* and data not shown). Many of the nuclei of passage 24–26 HGPS cells viewed at low magnification are extensively lobulated. Surprisingly, there is almost a complete loss of peripheral, and in many cases internal, heterochromatin in these nuclei (Fig. 3 *e* and *f*). Instead, these late-passage HGPS nuclei frequently contain a thick electron-dense lamina subjacent to the inner nuclear membrane (Fig. 3 *e* and *f*). This unusual electron-dense lamina is not evident in control cells. Furthermore, the distribution of pores in the envelopes of these late-passage cells is abnormal because they are clustered in small regions (data not shown). These latter observations correspond to those obtained by light microscopy (see Figs. 1 and 2).

On the basis of these results, we hypothesized that the increased concentration of LAΔ50 seen in later-passage HGPS cells (Fig. 1*f*) disrupts the normal processing, turnover, and assembly state of LA in the lamina. Specifically, we further hypothesized that these abnormalities may be caused by the loss of the second endoproteolytic cleavage site in LAΔ50, which is required for the conversion of normal pre-LA to LA. To test the possibility that LAΔ50 might be inhibiting the processing of WT pre-LA to LA, we used a pre-LA-specific Ab (see *Materials and Methods*). This Ab does not detect the band thought to represent LAΔ50 (Fig. 1*f* and data not shown). This lack of cross-reactivity is expected because the epitope (LA residues 647–660) is largely missing. The nuclei of control foreskin or AG09602B fibroblasts (from passages 2–17) typically exhibited a few nucleoplasmic foci
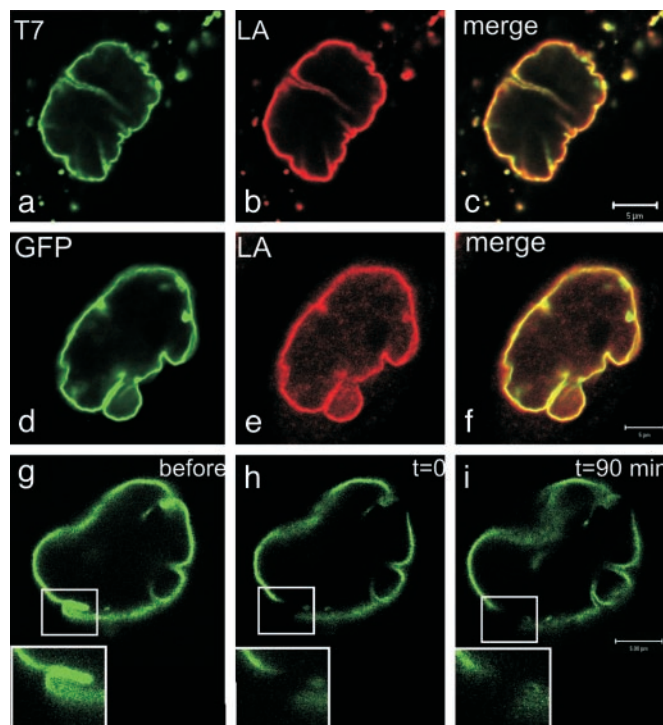

Fig. 4. The expression of LAΔ50 in normal cells causes rapid changes in nuclear shape. (*a*–*c*) A control AG09602 fibroblast double-labeled with anti-T7 tag and anti-LA 35 min after the microinjection of T7-tagged LAΔ50 into its cytoplasm. Before the injection of the live cell, phase-contrast microscopy revealed that the nucleus had a smooth surface and a normal ellipsoidal shape (not shown). (*d* and *e*) A highly lobulated nucleus of a HeLa cell 48 h after transfection with pEGFP-LA-Δ150 (*d*) and fixation and processing for indirect immunofluorescence with anti-LA (*e*). The overlay seen in *f* demonstrated that the endogenous LA and GFP-LAΔ50 showed extensive overlap. FRAP in the nuclear envelope region of a live HeLa cell after transfection with pEGFP-LAΔ150 showed that there was no detectable recovery after 90 min (*g*–*i*). The box in *g* indicates the area of interest just before photobleaching and is shown at higher magnification in the *Inset*. This area is shown immediately after bleaching (*h*) and at 90 min after bleaching (*i*). (Scale bars = 5 μm.)

with very little staining in the lamina region (Fig. 3*d* and data not shown). However, nuclei in HGPS cells from passages 6–13 exhibited more staining in both the nucleoplasm and lamina (Fig. 3 *a* and *b*), and by passage 26 the typically lobulated nuclei contained, in addition to nucleoplasmic foci, a brightly staining lamina (Fig. 3*c*). Immunoblotting of whole-cell extracts with pre-LA Ab showed a single band with increased intensity in later-passage cells (data not shown). Taken together, the data suggest that there is an increase in the number of WT pre-LA as the HGPS cells age in culture.

To more directly determine the role of the LAΔ50 protein, we injected bacterially expressed T7-tagged LAΔ50 (at a concentration of 1–2 mg/ml in injection buffer) into the cytoplasm of control foreskin fibroblasts (*Materials and Methods*). Cells selected for injection contained normally shaped nuclei. The mutant protein was rapidly transported into the nucleus and incorporated into the endogenous lamin network, including the lamina. After 30–35 min, many of the nuclei were similar to late-passage HGPS cells (Fig. 4 *a*–*c* and see Fig. 1). Cells that had been injected with the same concentration of T7 LA showed a similar time course of incorporation into the endogenous lamina but contained normal-appearing nuclei (19) (data not shown). This result showed that elevated levels of the mutant protein have a direct and immediate effect on nuclear shape independent of progression through the cell cycle. Attempts were also
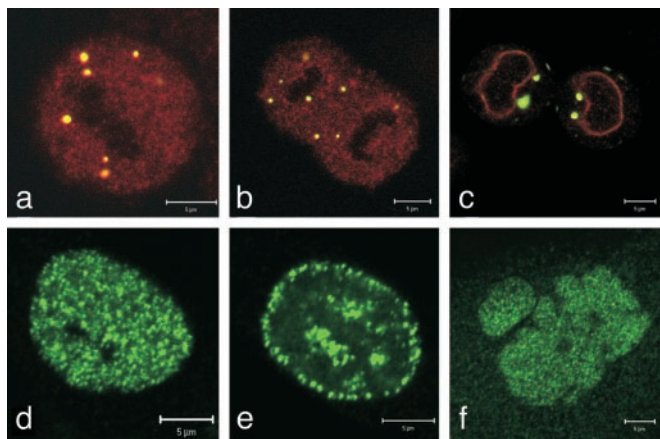
Fig. 5. The effects of the HGPS mutation on different stages of the cell cycle. Mitotic HeLa cells expressing GFP-LAΔ50 were fixed and stained for immunofluorescence with anti-LA (red). The GFP N-terminal tag appeared green. (*a*) A cell in the metaphase–anaphase transition showing that LA was diffusely organized throughout the cytoplasm because of its normal disassembly during mitosis, whereas GFP-LAΔ50 was seen mainly in large cytoplasmic aggregates. (*b* and *c*) The same types of aggregates remained in cells in telophase/early cytokinesis (*b*) and after daughter cell nuclei had reformed in early G₁ (*c*). (*d*–*f*) HGADFN003 cells processed for immunofluorescence with an Ab directed against proliferating cell nuclear antigen. Passage 6 cells with the typical pattern were seen in early (*d*) or mid-late (*e*) S phase, whereas *f* depicts the only pattern detected in a passage 26 cell containing a lobulated nucleus. This latter staining appeared similar to an early S-phase pattern. (Scale bars = 5 μm.)

made to "rescue" the mutant phenotype (extensively lobulated nuclei) in late-passage HGPS cells. This attempt involved the microinjection of WT T7-LA (see *Materials and Methods*), followed by fixation and processing for immunofluorescence. After 30 min we did not detect a significant change in nuclear lobulation (data not shown).

We also investigated the effects of the mutant LA protein by DNA transfection of HeLa cells. The majority of HeLa cells transfected with pEGFP-LAΔ150 and observed 24–48 h later contained highly lobulated nuclei that were similar to those seen in late-passage HGPS cells. Under these conditions, the GFP-tagged mutant protein colocalized with the endogenous LA (Fig. 4 *d*–*f*). FRAP analyses of the lamina in live HeLa cells expressing GFP-LAΔ50 showed no detectable fluorescence recovery after 90 min (Fig. 4 *g*–*i*). This finding is in contrast to FRAP experiments done in GFP-LA-expressing cells, which showed significant recovery within the lamina region after 60–90 min (data not shown; see ref. 12). We conclude that the interphase HeLa cell lamina was less dynamic with respect to subunit exchange compared with cells expressing only WT LA.

HeLa cells transfected with GFP-LAΔ50 were also observed in mitosis after fixation and staining with LA Ab. In metaphase/telophase cells, normal LA was disassembled and dispersed throughout the cytoplasm as expected (Fig. 5 *a* and *b*) (12). However, the GFP-LAΔ50 formed cytoplasmic aggregates, which remained even after the normal LA had entered the nucleus and formed a lamina in daughter cells (Fig. 5*c*) (12). Eventually, the GFP-LAΔ50 must enter nuclei to become incorporated into the lamin network, as cytoplasmic aggregates were not seen in typical interphase cells. We also carried out an analysis of S phase in HGPS cells by studying proliferating cell nuclear antigen patterns (25). From passages 6–13, typical early, mid-, and late S-phase patterns were readily detected (Fig. 5 *d* and *e* and data not shown). However, only nuclei resembling early S-phase punctate patterns were detected in passage 26 HGPS cells, suggesting a block in early S phase. It should be

noted that we have had great difficulty in growing HGADFN003 cells beyond passage 26.

Discussion

The results of this study demonstrate that there are progressive alterations in nuclear architecture in fibroblasts obtained from HGPS patients bearing the common *LMNA* mutation, 1824 C → T (6, 7). Although these cells are capable of expressing the mutant protein LAΔ50, their nuclei and lamina appeared normal at early passages, whereas at later passages their nuclei were severely misshapen and contained an abnormally thick lamina. In comparison, the majority of nuclei in the cells of an aged individual appeared normal even after many passages. In HGPS cells, the nuclear shape transitions were accompanied by a >2-fold increase in perimeter length and an ≈63% increase in cross-sectional area by late passages. These changes appeared gradually and were coincident with an increase in LAΔ50. This observation leads us to hypothesize that LAΔ50 rises as cells replicate and reaches a critical concentration, relative to normal LA, triggering a dominant-negative effect on lamin processing, assembly, turnover, and other changes in nuclear architecture. Further support comes from FRAP studies in HeLa cells expressing GFP-LAΔ50, in which fluorescence recovery rates in the lamina region were much slower than those obtained for GFP-LA (12). Furthermore, the microinjection experiments showed that a bolus of LAΔ50 rapidly induced lobulations in normal foreskin fibroblast nuclei, which were similar to those seen in late-passage HGPS cells. In contrast, attempts to restore the normal shape of highly lobulated nuclei by injecting WT LA into late-passage HGPS cells failed. These results suggest that the accumulation of LAΔ50 leads to an accumulation of WT pre-LA as a function of passage number, imposing a deleterious, stabilizing effect on the lamina/lamin network. The accumulation of both LAΔ50 and pre-LA could also be responsible for the changes in thickness of the lamina by inhibiting the processing of pre-LA to LA.

The severe alterations in nuclear shape in HGPS cells are consistent with the fact that lamins are directly involved in nuclear shape maintenance in interphase cells, and that nuclear shape changes are a hallmark for most laminopathies (8). The abnormal distribution of nuclear pore complexes seen in late-passage HGPS cells also is consistent with these observations, as it has been suggested that lamins anchor nuclear pores by means of their binding to NUP153 (26). Changes in the organization of nuclear pore complexes could therefore affect various aspects of the normal trafficking of protein and RNA across the nuclear envelope, causing severe effects on the physiological state of HGPS cells (27). The disruption of the normally close association between A- and B-type lamins seen in late-passage HGPS cells also could have deleterious effects on important nuclear functions. For example, it has been shown that the normal organization of LB is required for the chain-elongation phase of DNA replication (28, 29). Therefore, our finding that the highly lobulated late-passage HGPS cells exhibit proliferating cell nuclear antigen patterns resembling primarily early S phase suggests that there is a block in the transition from the early chain-elongation phase of DNA replication to the mid- and later phases of replication. This block could explain the premature cessation of growth in the later passages of HGPS cells. Another significant structural defect seen in late-passage HGPS nuclei is their loss of peripheral heterochromatin. This observation suggests that there are changes in the factors involved in gene regulation or silencing (30). This possibility is further supported by the findings that normal lamin organization is required for RNA polymerase II transcriptional activity and that transcription factors such as pRb and TBP (TATA-binding protein) are associated with lamins (31, 32).

The delayed targeting of GFP-LAΔ50 to HeLa cell nuclei after mitosis was not expected. This mutant protein contains a normal nuclear localization sequence (NLS), which is ≈180 residues upstream from the site of the 50-aa deletion in the common form of HGPS. Because it has been shown that WT LA is incorporated into nuclei immediately after the nuclear envelope assembles in daughter cells during early G_1 (12), this delayed entry of GFP-LAΔ50 may disrupt normal nuclear assembly and growth during this phase of the cell cycle. Such delays could also negatively affect the normal targeting and assembly of lamin-associated proteins such as LAP2α, a specific binding partner for LA (32). Because LAP2α binds to BAF (barrier to integration factor), a DNA-binding protein, the HGPS mutation could also affect the interactions between LA and chromatin (32). LAΔ50 may also inhibit the functions of numerous inner nuclear envelope transmembrane proteins known to interact with lamins (32). Other alterations in normal lamin functions due to LAΔ50 could be attributed to the loss or modification of phosphorylation sites. These include two potential cyclin-dependent kinase sites (Ser-652 and Ser-657) (33), which could alter various aspects of the cell-cycle-dependent regulation of lamin function. Furthermore, the second endoproteolytic cleavage site involved in the conversion of pre-LA to LA is lost in LAΔ50, which could produce a truncated, permanently farnesylated/methylated C-terminal cysteine. The presence of this form of LAΔ50 could have deleterious effects on the assembly, organization, and function of the lamins.

It is not possible to determine the precise mechanisms responsible for the premature aging process in HGPS patients at this time because this requires a much more extensive understanding of the structure and function of nuclear lamins and their potentially large number of binding partners. However, the results of this study support the hypothesis that the gradual accumulation of the defective product of the 1824 C → T mutation, in the presence of the WT *LMNA* allele, leads to serious defects in nuclear architecture and function. In the future, it will be of great interest to determine the relationships between the gradual changes in nuclear structure seen in cultured HGPS cells and the clinical features of this devastating disease.

1. Hutchinson, J. (1886) *Medicochir. Trans.* **69,** 473–477.
2. Gilford, M. (1904) *Practitioner* **73,** 188–217.
3. DeBusk, F. L. (1972) *J. Pediatr.* **80,** 697–724.
4. Baker, P. B., Baba, N. & Boesel, C. P. (1981) *Arch. Pathol. Lab. Med.* **105,** 384–386.
5. Stables, G. I. & Morley, W. N. (1994) *J. R. Soc. Med.* **87,** 243–244.
6. Eriksson, M., Brown, W. T., Gordon, L. B., Glynn, M. W., Singer, J., Scott, L., Erdos, M. R., Robbins, C. M., Moses, T. Y., Berglund, P., *et al.* (2003) *Nature* **423,** 293–298.
7. de Sandre-Giovannoli, A., Bernard, R., Cau, P., Navarro, C., Amiel, J., Boccaccio, I., Lyonnet, S., Stewart, C. L., Munnich, A., Le Merrer, M. & Lévy, N. (2003) *Science* **300,** 2055.
8. Goldman, R. D., Gruenbaum, Y., Moir, R. D., Shumaker, D. K. & Spann, T. P. (2002) *Genes Dev.* **16,** 533–547.
9. Weber, K., Plessmann, U. & Traub, P. (1989) *FEBS Lett.* **257,** 411–414.
10. Stuurman, N., Heins, S. & Aebi, U. (1998) *J. Struct. Biol.* **122,** 42–66.
11. Chen, L., Lee, L., Kudlow, B. A., Dos Santos, H. G., Sletvold, O., Shafeghati, Y., Botha, E. G., Garg, A., Hanson, N. B., Martin, G. M., *et al.* (2003) *Lancet* **362,** 440–445.
12. Moir, R. D., Yoon, M., Khuon, S. & Goldman, R. D. (2000) *J. Cell Biol.* **151,** 1155–1168.
13. Moir, R. D., Donaldson, A. D. & Stewart, M. (1991) *J. Cell Sci.* **99,** 363–372.
14. Spann, T. P., Moir, R. D., Goldman, A. E., Stick, R. & Goldman, R. D. (1997) *J. Cell Biol.* **136,** 1201–1212.
15. Moir, R. D., Montag-Lowy, M. & Goldman, R. D. (1994) *J. Cell Biol.* **125,** 1201–1212.
16. Davis, L. I. & Blobel, G. (1986) *Cell* **45,** 699–709.
17. Liu, J., Prunuske, A. J., Fager, A. M. & Ullman, K. S. (2003) *Dev. Cell* **5,** 487–498.
18. Yoon, M., Moir, R. D., Prahlad, V. & Goldman, R. D. (1998) *J. Cell Biol.* **143,** 147–157.
19. Goldman, A. E., Moir, R. D., Montag-Lowy, M., Stewart, M. & Goldman, R. D. (1992) *J. Cell Biol.* **119,** 725–735.
20. Starger, J. M., Brown, W. E., Goldman, A. E. & Goldman, R. D. (1978) *J. Cell Biol.* **78,** 93–109.
21. Smeulders, A. W. M. & Dorst, L. (1990) in *Manual of Quantitative Pathology in Cancer Diagnosis and Prognosis*, ed. Baak, J. P. A. (Springer, Berlin), pp. 77–104.
22. Wolff, N., Gilquin, B., Courchay, K., Callebaut, I., Worman, H. J. & Zinn-Justin, S. (2001) *FEBS Lett.* **501,** 171–176.
23. Östlund, C., Bonne, G., Schwartz, K. & Worman, H. J. (2001) *J. Cell Sci.* **114,** 4435–4445.
24. Vigouroux, C., Auclair, M., Dubosclard, E., Pouchelet, M., Capeau, J., Courvalin, J. C. & Buendia, B. (2001) *J. Cell Sci.* **114,** 4459–4468.
25. Sporbert, A., Gahl, A., Ankerhold, R., Leonhardt, H. & Cardoso, M. C. (2002) *Mol. Cell* **10,** 1355–1365.
26. Smythe, C., Jenkins, H. E. & Hutchison, C. J. (2000) *EMBO J.* **19,** 3918–3931.
27. Yoshida, K. & Blobel, G. (2001) *J. Cell Biol.* **152,** 729–740.
28. Spann, T. P., Goldman, A. E., Wang, C., Huang, S. & Goldman, R. D. (2002) *J. Cell Biol.* **156,** 603–608.
29. Kennedy, B. K., Barbie, D. A., Classon, M., Dyson, N. & Harlow, E. (2000) *Genes Dev.* **14,** 2855–2868.
30. Hall, L. L., Byron, M., Sakai, K., Carrel, L., Willard, H. F. & Lawrence, J. B. (2002) *Proc. Natl. Acad. Sci. USA* **99,** 8677–8682.
31. Mancini, M. A., Shan, B., Nickerson, J. A., Penman, S. & Lee, W. H. (1994) *Proc. Natl. Acad. Sci. USA* **91,** 418–422.
32. Shumaker, D. K., Kuczmarski, E. R. & Goldman, R. D. (2003) *Curr. Opin. Cell Biol.* **15,** 358–366.
33. Pearson, R. B. & Kemp, B. E. (1991) *Methods Enzymol.* **200,** 62–81.